ARTICLE

Surface Manipulation of Microtubules Using Self-Assembled Monolayers and Electrophoresis

John A. Noel,[†] Winfried Teizer,[†] and Wonmuk Hwang[‡,*]

[†]Department of Physics and [‡]Department of Biomedical Engineering, Texas A&M University, College Station, Texas 77843

ABSTRACT We integrate microtubule (MT)-resistant self-assembled monolayers (SAMs) with lithographically patterned electrodes to control MTs in a cell-free environment. Formed through a facile, one-step assembly method, the poly(ethylene glycol) trimethoxysilane SAM prevents MT adsorption on both silicon substrates and Au microstructures without casein. We characterize the SAM using ellipsometry, X-ray photoelectron spectroscopy, and atomic force microscopy and compare it with other MT passivation techniques. The SAM retains its passivating ability when used as a substrate for electron beam lithography, a key feature that allows us to pattern microtubules on lithographically defined Au structures. Moreover, by combining the SAM-passivated Au microelectrodes and DC electrophoresis, we demonstrate reversible trapping of MTs as well as capture and alignment of individual MTs.

KEYWORDS: protein patterning · self-assembly · tubulin · kinesin · biofouling · bioNEMS

Harnessing the dynamic functions of microtubules (MTs) provides a method for building hybrid nanobiosystems from the bottom up. MTs are a major structural component in cells and nerve fibers and are essential for cell division, cell motility, and vesicle transport. MTs are also a target for treatment of cancer and Alzheimer's disease.[1,2] Interest in MTs stems not only from the vital functions they perform in the cell but also from their ability to act as nanoscale shuttles driven by motor proteins, as scaffolds for guided assembly of nanoparticles, and as a basis for synthesizing nerve-like systems.[1,3,4]

A natural way for developing MT-based hybrid systems is by using engineered surfaces, where ideally one would be able to externally control the location, orientation, and even polymerization of the MTs. More generally, to establish surface control of biomolecules, two major issues must be addressed: (1) preventing undesirable adsorption, or fouling, and (2) immobilizing or otherwise confining the target biomolecules to predefined regions. Of these two goals, the former is a prerequisite to the latter, as the fouling is often irreversible in the laboratory time frame and may dominate over targeted immobilizations at the micro- or nanoscale. Because MTs tend to adhere strongly to glass and silicon surfaces, the milk protein casein is frequently used for surface passivation.[3] However, passivation using poly(ethylene glycol) (PEG) organosilanes has several advantages over casein. First, the noncovalent interaction that binds caseins to the silica surface is considerably less stable than the covalent bonds of grafted organosilanes. This increased stability, as well as the ability of organosilanes to form ordered, smooth surfaces makes them more suitable as substrates for lithographic patterning. Second, the mechanism through which grafted layers prevent protein adsorption has been studied in much detail, providing several models through which one can analyze the interaction between MTs and grafted organosilanes.[5] In contrast, the passivation mechanism through which casein prevents protein adsorption is not well-understood.[6] We have quantitatively analyzed the extent to which casein and PEG SAMs are able to prevent MT fouling on glass and silicon and compare these with two other common passivating methods: hydrophilization and surfactants. The methods chosen for study have been shown to reduce biomolecule adhesion in a variety of settings, though, to our knowledge, PEG-functionalized SAMs, which prevent MT fouling without casein, have not been previously reported.[7−10]

Once surface fouling of MTs has been prevented, immobilization may be attempted. Surface immobilization of proteins, DNA, cells, and microspheres has been achieved through nonspecific adsorption, ligand-receptor binding, and chemical cross-linking.[11−15] Several studies have successfully employed these methods for im-

*Address correspondence to hwm@tamu.edu.

Received for review March 31, 2009 and accepted June 05, 2009.

Published online June 11, 2009.
10.1021/nn900325m CCC: $40.75

© 2009 American Chemical Society

mobilizing MTs.[7,16,17] While these methods are suited to assays of adsorption kinetics and related phenomena, they do not provide for external control of the onset and duration of target binding. This is because the surface begins binding the target molecules immediately after their introduction, which precludes the on-demand, reversible manipulation that we seek. Additionally, several works have made use of the highly specific interaction between MTs and the motor protein kinesin to immobilize and orient MTs in microfluidic channels and on planar surfaces.[3,18,19] In these studies, surface-bound kinesins were used to capture and bind MTs while casein was used to passivate the surface against MT adsorption. In addition to suffering from the same lack of external control mentioned above, large proteins such as kinesins are not ideally suited as robust surface linkers that can withstand changes in environmental conditions. To provide such active manipulation and on-demand adsorption, we employ DC electrophoresis. Electrohydrodynamic forces such as DC electrophoresis are compatible with MTs, programmable, and readily incorporated into electrochemical sensor assemblies.[20−24]

We show that PEG-silane SAMs can be made to prevent MT adsorption effectively and then integrate these SAMs with gold structures patterned through electron beam lithography (EBL). The integration of the SAM with lithographic patterns demonstrates that the SAM is useful as either a nonfouling substrate or overlayer onto which MTs can be reversibly assembled and oriented using DC electrophoresis. The technique has a distinct advantage over methods which employ chemical binding or protein-ligand cross-linkers (such as biotin and streptavidin) and does not require fabrication of microfluidic channels to confine the MTs.[18,25,26] More broadly, the combination of SAM, EBL, and electrical manipulation has the potential for making functional nanopatterns of biomolecules.

RESULTS AND DISCUSSION

Microtubule Antifouling Surfaces. Fouling of fluorescently labeled MTs onto glass and silicon substrates treated with hydroxylation, Triton X-100 surfactant, a PEG SAM, or casein was measured using fluorescence microscopy. MT adsorption to cleaned glass and silicon surfaces was used as a control. A flow chamber was assembled from the test surface and a glass coverslip, and the solution of MTs was introduced into the chamber, then flushed out (Figure 1a). The untreated glass coverslip at the bottom of the chamber in each assay served as a reference that allowed us to quantitatively compare the fouling on the different test surfaces (Figure 1b).

The results, reported in Table 1, indicate that the SAM and casein passivate silicon surfaces extremely well, while Triton X and hydrophilization worked well on glass but not as well on silicon. As expected, the MT

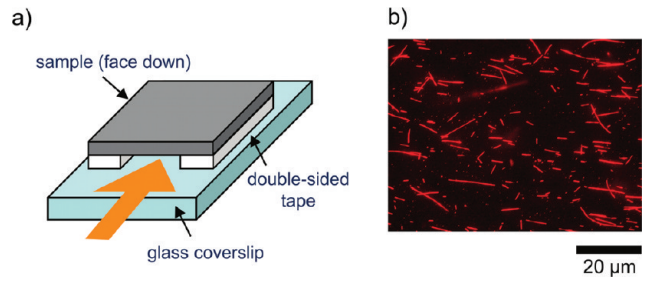

Figure 1. Passivation assay setup and fouling of MTs. (a) Flow cell with inverted sample mounted to a glass coverslip. Large arrow indicates direction of fluid flow. (b) MT fouling on a clean glass coverslip.

adsorption to the casein-passivated surface was below the level of fluorescence detection.

We used Triton X to passivate the flow cell prior to MT injection and also included it in the MT solution at 0.05% v/v. Compared to the nonspecific adsorption on clean silicon substrates, this method was moderately successful in reducing MT adsorption, with area coverage of 66% of the value for clean glass. However, as with the hydrophilization, Triton X was much more successful at reducing MT adsorption on glass substrates, resulting in 12% as compared to the clean glass.

PEG SAMs have been shown to be quite stable and exceptionally resistant to protein fouling. van den Heuvel *et al.* successfully incorporated a PEG SAM onto engineered surfaces for rectifying MT-kinesin motility and studying MT docking to kinesin-covered electrodes.[22,27] Because, in those reports, casein was used in addition to the SAM, we studied the ability of the SAM alone to resist MT adsorption, which was found to be comparable to casein, with over 99% MTs blocked (Table 1). SAMs prepared in this way are quite robust as they can be flushed clean, dried, sonicated in organic solvents, and reused without loss of nonfouling properties, which would be difficult to achieve using noncovalently bound proteins such as caseins. Furthermore, a wide choice of SAM molecules allows for additional functionalization of the surface.

Although substrate hydrophilization and surfactants show MT resistance, they are not suitable for creating binary surfaces because they make poor substrates for micro- and nanofabrication and because methods for geometrically restricting them on the surface are not well-developed. Casein is used in most cell-free MT studies because it passivates a variety of surfaces to MT adsorption including glass, silica, gold, and SAMs. Interestingly, casein which has been subjected to

TABLE 1. Assaying Passivation of Silicon and Glass to MT Adsorption[a]

	clean	hydrophilic	Triton X	PEG SAM	casein
silicon	0.8620 ± 0.1423	0.7927 ± 0.1312	0.6589 ± 0.0909	0.0079 ± 0.0082	0
glass	1.0000 ± 0.3087	0.1772 ± 0.0776	0.1181 ± 0.0237	N/A	0

[a]Values reported as area covered by MTs relative to clean glass (see Methods). No MTs were detected on casein-coated surfaces. No value is given for SAM passivation on glass as we did not attempt to form SAM layers on glass substrates.

lithographic resist coating and removal retains its antifouling ability in kinesin motility assays.[28] Yet the detailed mechanism for casein passivation is not well-understood.[6,29] It does not have well-defined secondary or tertiary structures and is relatively hydrophobic, so it tends to form micelles of various shapes and sizes.[6] Consequently, casein coatings will thus be thick and have high roughness, and caseins may easily detach and reattach to the surface. Strong blocking by casein thus could be simply the result of detachment of caseins loosely bound to the surface as they nonspecifically attach to MTs.

MT-Resistant Trimethoxysilane SAM. To understand the mechanism behind the MT resistance of the SAMs, we further characterized the SAM using ellipsometry, angle-resolved X-ray photoelectron spectroscopy (ARXPS), and atomic force microscopy (AFM). These methods are able to determine the thickness, morphology, and roughness of the SAM.[5] From ellipsometry, the SAM thickness was determined to be 3.26 $\pm$ 0.66 nm, where the error is the standard deviation across three different regions.[30,31] The ARXPS measurements on identically prepared samples resulted in a SAM thickness of 3.35 $\pm$ 0.27 nm. Tapping mode AFM, carried out in ambient conditions, was used to scan a minimum of four 1 $\times$ 1 μm^2 regions on two samples for both the bare silicon and the SAM. Care was taken to avoid spurious topographic data by comparing vertical and horizontal scans of each region and also by periodically comparing feature sizes obtained from smaller, high-resolution scans to those obtained at 1 $\times$ 1 μm^2. Using a silicon probe with a nominal tip radius of 8 nm, the average of the root-mean-square roughness, R_{rms}, was determined to be 0.51 $\pm$ 0.10 nm, indicating a smooth, homogeneous silane layer, consistent with previous AFM studies on similar PEG SAMs.[32,33] By comparison, the bare silicon substrate measured under the same conditions had R_{rms} = 0.14 $\pm$ 0.01 nm. The SAM may have higher roughness because the SAM molecules, although densely packed, are not maximally packed to a crystalline order (see below), so they are not perfectly stretched in the thermally fluctuating environment. Polydispersity in the length of SAM molecules (3.0−3.8 nm) may also have contributed to the roughness, which is comparable to R_{rms} of the SAM. On the other hand, as verified by the topography image of the AFM and by low variability in height measurements (see Methods), the roughness is not likely due to patchiness or island formation with low surface coverage, which may transiently occur during the early stage of SAM growth.[33]

The thickness of the PEG SAM is close to that found for SAMs formed from analogous PEG-thiol molecules prepared under similar conditions, although it is somewhat thicker than layers formed using vapor deposition and a lower concentration solution method (as opposed to the high-concentration method used herein).[31,32,34,35] The thicker SAM presented here is likely due to the high solution concentration and long incubation time, which tend to increase the surface density of the silanes and extend the flexible PEG chains into a brush-like conformation (discussed below).[9]

Although the mechanism behind the protein-resistant properties of the PEG-silanes is not fully understood, several factors have been shown to explain the observed phenomena including steric repulsion by the flexible PEG chain, distal chemistry and surface density of the grafted molecule, and surface hydration.[36−38]

We estimated the surface density of silane molecules using the SAM thickness (d):

$$\sigma = nd$$

where σ is the number of molecules per unit area and n is the number density. Using Avogadro's number (N_A), the bulk density of the PEG-silane molecule (ρ = 1.08 g/cm^3), and its molecular weight (M_W = 450−600 g/mol), we determined n:

$$n = \frac{N_A \rho}{M_W}$$

The range of molecular weights of the PEG-silane molecule gives the surface density of the SAM as 3.53−4.71 molecules/nm^2. This is 61−81% of the close packed maximum, 5.8 molecules/nm^2, indicating a densely packed monolayer.[34,37] The high surface density and the fact that the PEG-silane molecule has a length of 3.0−3.8 nm, approximately the thickness of the SAM, indicate a brush-like arrangement of the PEG chains.[39]

The method used for the SAM preparation (a long, liquid phase formation at elevated temperature) likely results in a single siloxane bond formed from one of the methoxy head groups, while the other two methoxy groups either remain intact or cross-link to neighboring silanes.[40,41] This would present a disordered layer of methoxy and cross-linked silanes near the silicon surface in addition to the distal methoxy group and may explain the high resistance to MT adsorption; a diagram of this proposed SAM structure is presented in Supporting Information Figure S1. Because distal methoxy groups are likely present at the solution interface, it is evident that these groups do not promote MT binding.

Integration of SAM with Electron Beam Lithography. As a demonstration of the versatility of this approach for patterning functional surfaces for biomolecules, we have integrated the SAM with lithographic patterns. Due to the robust nature of the SAM, the procedure is straightforward. Two methods were used depending on whether the nonfouling SAM layer would be below or above the lithographic pattern, referred to as "passivated" and "unpassivated" electrodes, respectively (Figure 2). The SAM preparation described above was used for both methods. The unpassivated electrode was fab-

ricated by first forming the SAM on the silicon substrates, then spinning on polymethylmethacrylate (PMMA) resist and continuing with standard positive tone EBL (Figure 2a). The passivated electrode was fabricated by first making a gold pattern on the silicon substrate and then overlaying with a SAM (Figure 2b). MT patterning experiments, discussed below, showed that the SAM was able to retain its high resistance to MT fouling in both unpassivated and passivated configurations.

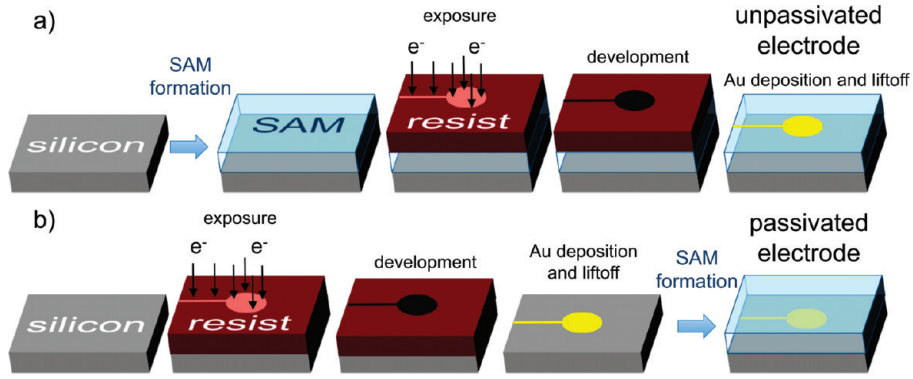

Figure 2. Fabrication of (a) an unpassivated electrode on a passivated silicon substrate and (b) a passivated electrode using a SAM overlayer. Standard positive tone electron beam lithography steps are shown. Disc-shaped electrode with electrical connection is shown in gold. Not to scale.

The unpassivated electrode presents a surface with binary properties: unpassivated Au with a higher affinity for MTs and the adjacent low-affinity SAM region. Because the Au remains exposed, MTs nonspecifically adsorb to the Au upon introduction to the flow chamber (Figure 3). However, a wide variety of additional modification can be achieved by using the Au pattern as a template for thiol functionalization, although we do not explore it in this study.[42] For the passivated electrodes, no MT fouling was seen on 60 μm diameter Au disk patterns, although we did observe MT adsorption on larger patterns (>100 μm). Despite silicon dioxide surfaces being used most often for silane SAM formation, these SAMs are known to cross-link laterally, as discussed above, which may explain the ability of the SAM to passivate the smaller gold patterns (Figure S1 in Supporting Information).[41] Interestingly, these results indicate that the size of the underlying Au microstructure affects the formation of the SAM layer. Under the condition used in this study, the absence of covalent coupling of the silane to the Au surface appears to disrupt the SAM formation only for the larger diameter Au structures, though further study is required to fully understand this phenomenon. Below, we employ passivated patterns for on-demand electrophoretic adsorption of MTs.

Reversible Trapping of Microtubules Using Electrophoresis. To externally direct MT localization, we applied a DC potential across the flow cell to induce electrophoretic migration of the MTs. This allows us to prevent MT fouling on the Au surfaces prior to application of the DC potential, and in this way, the passivated Au patterns are used as templates for on-demand MT adsorption, rather than relying on passive adsorption as in Figure 3. Because the isoelectric point of tubulin is approximately 5.4, the MTs are negatively charged when suspended in a buffer at pH 6.8. Upon application of a potential, the MTs migrate to the lithographically patterned gold, which acts as the anode (Figure 4). A glass coverslip coated with Cr and Au (2 and 4 nm, respectively) was used as the counter electrode. The ultrathin counter electrode transmits light, allowing the patterned surface to be imaged through it. Since the counter electrode was not passivated, a small amount of MTs fouled on the surface, but they are out of focus and do not interfere with the imaging of the passivated pattern (Figure 4, bottom). Rather, the faint fluorescence of the fouled MTs often aided in locating the passivated Au patterns prior to application of the potential. Using a DC power supply, potentials up to 1.5 V were applied vertically through the flow cells with approximately 60 μm between the electrodes. Above about 1.2 V, the likelihood for formation of gas bubbles (due to electrolysis) and MT depolymerization increased dramatically.

On demand, reversible MT adsorption is shown in Figure 5 and Supporting Information Video 1 for a 60 μm passivated disk electrode. After introduction of MTs, we sealed the open ends of the flow cell with nail

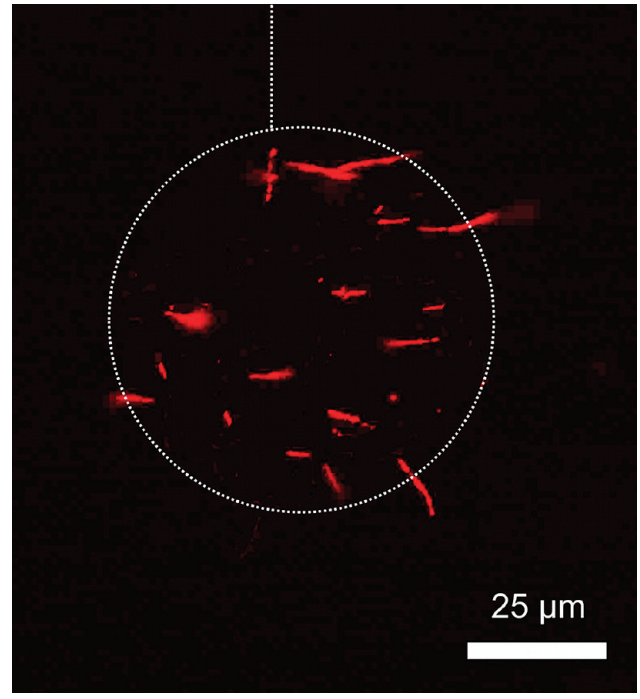

Figure 3. Nonspecific adsorption of MTs to a bare (unpassivated) gold pattern. Absence of fouling in surrounding regions demonstrates the ability of the SAM to retain its passivating properties through lithographic processing.

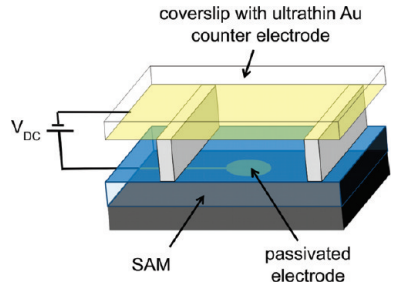

Figure 4. Flow cell with electrodes for electrophoretic control of MTs. Ultrathin counter electrode passes light for imaging MT patterns with fluorescence microscope. Objects not shown to scale.

polish to prevent lateral fluid flow due to evaporation. Prior to application of the potential, there is no adsorption of MTs on either the electrode or the substrate due to the passivating monolayer (Figure 5a). Remarkably, even those MTs that are very close to the electrode are seen to be unattached and are mobile, indicating that the SAM layer effectively passivates the electrode (Supporting Information Video 1).

When the potential is switched on, MTs migrate to the anode, localizing at the pattern while the surrounding regions remain free of MTs (Figure 5b). The MTs that are in focus are located very near the plane of the disk electrode. Upon reversal of the potential, the MTs are driven away from the pattern (Figure 5c). This process of reversible adsorption, or trapping, can be repeated until the MTs begin depolymerizing from fluorescence exposure (approximately 30 min), making it possible to switch the pattern between "MT on" and "MT off" states. The thermal motion of the MTs, which can be seen in Supporting Information Video 1, indicates the absence of fouling on the electrode.

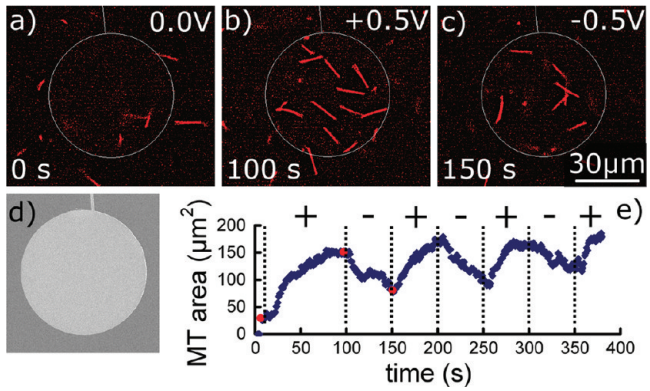

Figure 5. Reversible MT adsorption on a passivated disk electrode. (a) Initially, the electrodes are grounded, and there is no adsorption. (b) MTs are concentrated on the disk for 100 s at +0.5 V DC. (c) Potential is then reversed to drive MTs away for 50 s. White lines indicate edges of electrode. (d) Scanning electron microscopy (SEM) image of a disk electrode. (e) Plot of MT area in μm² (converted from pixel area) covered by MTs on the electrode as a function of time with +0.5 and −0.5 V applied alternately; images a−c are taken from the same experiment and are indicated in the plot with a red dot. See Supporting Information Video 1 for the time compressed image sequence showing the motion of the MTs.

Despite application of the positive and negative potentials for equal time, a gradual increase in the number of MTs can be seen near the electrode even though the surface continues to remain free of fouled MTs. This can be seen in Figure 5e when comparing the MT coverage at 150, 250, and 350 s. This hysteretic behavior may be due to the nearby surface inducing a higher drag coefficient for MTs moving away from the electrode, as opposed to the bulk drag coefficient that applies during attraction (Figure S2 in Supporting Information).[43] In other words, it appears that MTs are more easily attracted to the surface than driven away. Further studies are necessary to better understand the behavior of the MTs as well as the buffer ions near the electrode and MTs. However, if it is necessary to clear MTs off of the electrode, they can be easily flushed away by external flow during the voltage reversal phase, which can be done by connecting a pump to the sealed flow cell.

Template Patterning of MTs and Single MT Orientation. This method of reversible, at-will MT adsorption may prove useful for guiding MTs to assemble into more organized filamentous structures. Toward this end, we tested the ability of this device to capture and align MTs on narrow gold electrodes. We found that high aspect ratio passivated electrodes are able to orient MTs to the shape of the pattern after the filaments reach the surface (Figure 6 and Supporting Information Video 2). Lines and rings were fabricated with line widths of 1 μm, and a potential was applied as above. As with the disk electrode, there was no MT adsorption prior to application of the potential (Figure 6b). Upon application of 1 V, MTs rapidly adsorb at high density along the line at the top of the ring and tangent to the ring itself (Figure 6c−e and Supporting Information Video 2).

Because the MTs begin to overlap very quickly, it is difficult to determine the extent of this alignment. To observe the adsorption process more closely, we reduced the MT concentration by one-half (12.5 nM final tubulin concentration) and repeated the experiment. Figure 7 is a series of images that show the adsorption and alignment of a single MT to the same size ring electrode as in Figure 6 (shown at higher magnification). The images are all focused in the plane of the gold pattern. The MT is out of focus at 2.68 s and

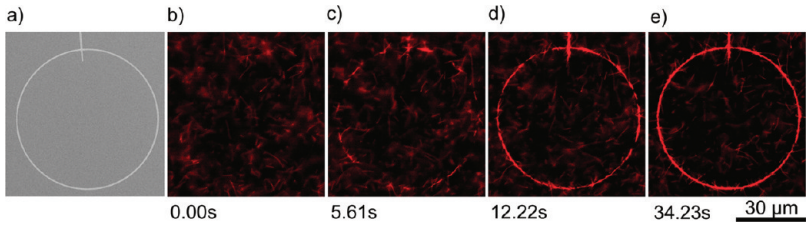

Figure 6. MT adsorption and alignment on a ring electrode. (a) SEM image of ring electrode. The Au ring has a line width of 1 μm and a diameter of 60 μm. (b−e) Time course of MT adsorption after +1.0 V is applied to the electrode at 0.00 s. A tubulin concentration of 25 nM was used. See Supporting Information Video 2.

comes into focus as it adsorbs to the ring at 4.20s, while the area surrounding the electrode remains free of MT fouling (Supporting Information Video 3).

These results indicate that MTs are able to quickly align on the electrode surface once the potential is applied. We postulate that the low interaction of the MT with the SAM layer on the passivated electrode promotes this high degree of orientation (as compared to the unpassivated gold) as it allows the MT to reposition after making initial contact with the surface. It should be noted that the smaller the gold pattern, the higher the potential required for inducing electrophoretic motion of the MTs. As a result, many of the MTs adsorbed to the ring electrodes in Figures 6 and 7 remain after the potential is reversed. This higher potential exerts a larger force on the MTs that may be strong enough to overcome the steric repulsion of the SAM or to deform the SAM itself by altering the brush-like configuration of the PEG chains.[36,44] It is also possible that the field locally destroys the SAM, although this is unlikely since depolymerization of MTs, despite being less stable than the SAM, was pronounced only at high field strength. In effect, the MT resistance of the SAM is switched off by the application of the higher field, a feature that may allow for immobilization of short "seed" MTs to small patterns that can then be elongated by addition of free tubulin. In this way, it may be possible to "grow" polar MT structures after immobilization on the template. Additionally, by growing MTs on the surface and stopping when MTs reach appropriate lengths, it will be possible to avoid steric interactions between MTs that may prevent some filaments from completely aligning on the electrode (bottom of the arc in Figure 7).

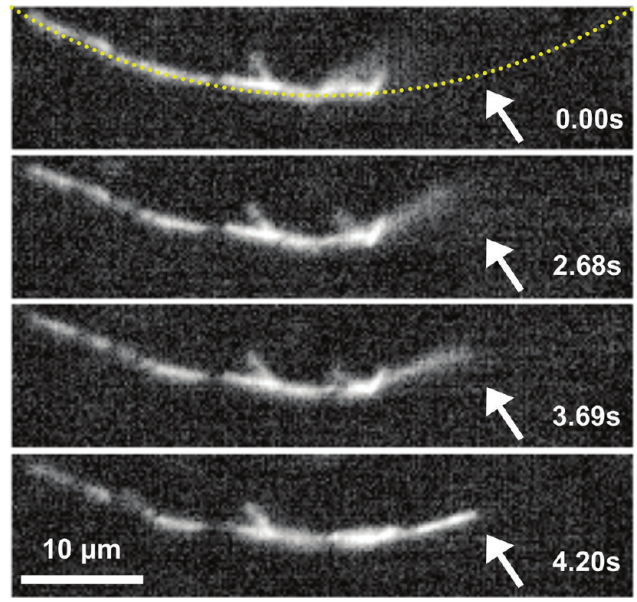

Figure 7. Individual microtubules aligning on a ring electrode with +1.2 V applied. The dotted line indicates the path of the underlying gold electrode. Time elapsed from the first frame is given in seconds. White arrow indicates a single MT adsorbing to the ring.

CONCLUSION

Among several methods tested for passivating glass and silicon surfaces against MT adsorption, we found that the organosilane PEG SAMs have the most desirable qualities: a high resistance to MT adsorption, compatible with EBL, and simple to prepare. The facile SAM preparation method, which uses a commercially available PEG-silane, has been shown to prevent 99.2% of MT adsorption as compared to clean glass. Characterization of the SAM using ellipsometry, ARXPS, and AFM allows us to estimate the surface density of the silane molecules and thus the orientation of the molecules in the monolayer. The MT resistance is likely due to a high density of cross-linked PEG-silane molecules that present low interacting methoxy groups at the solution interface. These results on the interaction of protein filaments with nonfouling SAMs complement previous studies which used smaller globular proteins.[36]

The robust nonfouling SAM was successfully integrated with EBL for controlling *in vitro* MT-surface interactions. We determined that the SAM retained its passivating properties after lithographic patterning. When the SAM overlaid the lithographic patterns, the passivated electrode was used to produce on-demand, reversible MT trapping. Furthermore, single filaments were shown to orient in a parallel fashion onto electrodes in the form of gold lines and circles 1 μm in width, though controlling MT polarity remains a goal for future work.

Furthermore, we use standard EBL to pattern *on* the SAM as opposed to more laborious methods which focus on controlling the location of the SAM molecules.[45] For both the unpassivated and passivated electrodes, the size and geometry of the gold patterns are limited only by the capabilities of the EBL system, with the smallest attainable features currently at about 10 nm, the same scale as single proteins.

This method bridges the gap between nanoscale and mesoscale assembly of biomacromolecules on synthetic surfaces and is applicable to studies ranging from cell-free axonal transport models to biosensor technology. More generally, the electrophoretic technique may be used for patterning many different proteins because, like MTs, most proteins carry a native charge. Additionally, methods for cross-linking biomolecules to alkanethiol SAMs on gold are well-developed and are capable of presenting a variety of functional surface groups on the unpassivated gold pattern.[42] In order to assemble MT structures that mimic those found in cells, further work must be carried out to control MT−MT interactions and orient the MTs in an isopolar fashion. This may be possible through integration of kinesin motors and other MT-associated proteins with the on-demand patterning and manipulation techniques presented here, ultimately providing a foundation for cell-free assembly of MT-based superstructures.[3]

METHODS

Materials. SAMs were made using 2-[methoxypoly(ethyleneoxy)propyl]trimethoxysilane (PEG-silane), 95%, from Gelest, Inc. High-purity, lyophilized bovine brain tubulin (unlabeled and rhodamine labeled) was purchased from Cytoskeleton, Inc. A nonhydrolyzable guanosine nucleotide (GMPCPP) was used for MT polymerization (Jena Biosciences, GmbH). Triton X-100, ethylene glycol bis(2-aminoethylether)-*N*,*N*,*N*′,*N*′-tetraacetic acid (EGTA), glucose oxidase, peroxidase, glucose, 2-mercaptoethanol, piperazine-*N*,*N*′′-bis(2-ethanesulfonic acid), taxol, hydrogen peroxide (30%), and sulfuric acid (96%) were purchased from EMD Chemicals. Isopropanol, acetone, toluene, and chlorobenzene were all ACS grade and obtained from EMD Chemicals. Polymethylmethacrylate (PMMA, molecular weight 950 kDa) was obtained from Brewer Scientific. Methylisobutylketone (MIBK, ACS grade) was obtained from Fisher Scientific. No.1 borosilicate glass (referred here simply as "glass") coverslips (22 × 50 mm) were purchased from VWR. Polished electronic grade p-type ⟨111⟩ silicon (referred here simply as "silicon") wafers were purchased from Addison Engineering, Inc.

Microtubule Preparation. The following MT preparation procedure was adapted from the lab of Tim Mitchison at Harvard. Rhodamine-labeled tubulin (50 μM) was mixed with unlabeled tubulin (50 μM) at a ratio of 1:2 in PIPES buffer (80 mM piperazine, 1 mM $MgCl_2$, 1 mM EGTA, pH 6.8 with KOH) containing 5% glycerol and 1 μM GMPCPP. The tubulin was allowed to polymerize at 37 °C for 30 min then diluted to a concentration of 0.5 μM in PIPES buffer supplemented with 20 μM taxol. Before each assay, an oxygen scavenging cocktail (glucose 45 mg/mL, glucose oxidase 2 mg/mL, catalase 0.35 mg/mL, 2-mercaptoethanol 5% v/v in PIPES buffer) was freshly prepared and added to the MTs to prevent depolymerization from fluorescence excitation. The final tubulin concentration used was 0.45 μM unless specified otherwise.

Passivation Assay. To assay passivation of sample surfaces, fluorescently labeled taxol-stabilized MTs (approximately 45 nM tubulin concentration) were flushed into flow cells assembled by fixing the treated sample surface face down onto a cleaned glass coverslip using double-sided tape (Figure 1a). Solutions were pipetted into one end of the flow cell, while a Kimwipe was used to wick the solution out of the other end. The typical volume of the flow cell was about 4 μL. In experiments that required displacement of one solution with another, we flushed in 40 μL of each additional solution to ensure a complete volume exchange. Because each flow cell was assembled by the juxtaposition of a clean glass coverslip and a test surface in different focal planes, we were able to examine and compare both surfaces concurrently. After allowing the MTs to adsorb for 5 min, the unattached MTs were flushed out with 40 μL of PIPES buffer supplemented with an oxygen-scavenging solution. The MT adsorption was observed at 60× magnification under a Nikon TE2000 microscope equipped for fluorescent imaging. The amount of MT adsorption was surveyed by capturing images of 10 different regions distributed across each surface. Using the NIS-Elements software (Nikon, Inc.), the total pixel area covered by MTs was tabulated. In each assay, the adsorption of MTs to the clean glass coverslip was monitored as a control in order to prevent errors arising from sample-to-sample variation in fluorescence intensity and MT concentration. The values reported in Table 1 were scaled to the value for the clean glass substrate in each passivation assay (Figure 1a), except for the Triton X assay, where the clean glass value was measured in a surfactant-free solution of MTs. Error was tabulated from the standard deviation of MT coverage across all 10 images captured for each assay.

Hydrophilization. Glass substrates were made hydrophilic by hydroxylation with Piranha solution (hydrogen peroxide in sulfuric acid, 1:4, v/v). *Warning: piranha solution is extremely reactive and poses an explosion hazard.* The substrates were first cleaned with the standard cleaning procedure, as referred to in this work, which consists of sonication of fresh substrates in acetone for 5 min followed by rinsing with isopropanol and drying with nitrogen gas. They were then immersed under fresh Piranha solution, which was hot due to the exothermic reaction from mixing, for 10 min followed by rinsing with deionized water and drying with nitrogen gas. The substrates were then rinsed with 0.1 M KOH for 10 s followed by a rinsing with DI water and drying under nitrogen.[7]

Casein Protein Passivation. Casein was used to passivate the surfaces in the same manner as standard motility assay protocols.[46] A "blocking" solution of 0.05 mg/mL casein in PIPES buffer was flushed into the flow chamber, which was assembled as above using a cleaned silicon wafer as the sample surface. The casein was allowed to passivate the surfaces for 5 min, and then the MT solution, which has been supplemented with 0.2 mg/mL casein, was flushed into the chamber and the remainder of the assay carried out as above.

Surfactant Treatment. Triton X-100 surfactant was used to passivate surfaces in the same way as casein. A blocking solution containing 0.05% v/v Triton X-100 in PIPES buffer was flushed into the flow chamber and left for 5 min. Triton X-100 at 0.05% was also added to the MTs before they were flushed into the chamber. The remainder of the assay was performed as above.

PEG SAM Preparation. PEG-silane was mixed to 5% v/v in toluene and stirred for 1 min. Silicon substrates, 8 to 10 pieces cut to approximately 1 cm × 1 cm, were cleaned with the standard procedure (in the hydrophilization section above), placed in the bottom of a 250 mL glass beaker, and covered with 20 mL of the SAM solution. The beaker was placed in a ventilated oven at 75 °C for 21 h. After removal from the oven, a viscous residue of PEG-silane covered the wafers and the bottom of the beaker. The substrates were rinsed vigorously with toluene, then rinsed with isopropanol and dried with nitrogen gas. Passivation assays were carried out as described above. This protocol was adapted from Papra *et al.*,[32] but we did not perform additional surface oxidation in Piranha prior to SAM formation, and the SAM was formed without hydrochloric acid in the SAM solution.

Ellipsometry. Ellipsometry was carried out on a Nanofilm EP 3-SE ellipsometer. Using the vendor software, the ellipsometry data were fit to a three-layer model (air, film, substrate) under the assumption that both the SAM and the silicon oxide are thin and transparent and have an index of refraction of 1.46.[30,31] The average thickness and its standard deviation of the SAM was determined from measurements of three regions on each sample (3.26 ± 0.66 nm).

Angle-Resolved X-ray Photoelectron Spectroscopy. ARXPS was used to measure the presence of the SAM layer and to provide a second measurement of the SAM thickness. PEG SAMs were prepared as described above. Measurements were carried out using a Kratos Axis Ultra photoelectron spectrometer with a monochromated Al Kα (1486.6 eV) source. All measurements were made at pressures lower than 2×10^{-7} Torr. Data, including peak intensity and elemental composition, were analyzed using the vendor software. To verify the grafting of the SAM onto the substrates, three areas on each sample were analyzed with survey scans over a range of binding energy from 0 to 1400 eV. High-resolution scans of O 1s, C 1s, and Si 2p regions were also made. The analyzer was oriented at an angle of $\theta = 0°$ from the surface normal for these measurements. Thickness measurements were made by varying θ from 0 to 75°.[47]

Atomic Force Microscopy. We used Veeco CP II AFM to determine the surface roughness and morphology of the SAM and silicon substrates. Tapping mode AFM was used in ambient air at driving frequencies ranging from 70 to 90 kHz. Cantilevers were antimony-doped silicon with a spring constant of 15 N/m and nominal tip radius of 8 nm (FESP model from Veeco Probes). We scanned a minimum of four regions on two samples for both the bare silicon and the SAM. The range of height values was considered to confirm that there was a low variability in the height of surface features, which indicates a smooth surface, a characteristic that can be overlooked by only analyzing R_{rms}.

Electron Beam Lithography. All patterns were fabricated using positive tone EBL. Silicon wafers with native oxide were cut to approximately 1 × 1 cm^2 and cleaned using the standard acetone/ isopropanol procedure outlined above. Electron-beam resist (PMMA, 3% w/v in chlorobenzene) was spun onto the wafers (4000 rpm for 40 s) then cured on a hot plate at 160 °C for 90 s. A JEOL electron microscope equipped with NanoPattern Generating Software controllers (JC Nabity) was used for e-beam writing. After exposure, patterns were developed with MIBK in

isopropanol (1:3) for 70 s followed by thermal vapor deposition of a 3 nm chromium adhesion layer and 12 nm of gold. The substrates were then placed in acetone for 30 min, which lifted off the remaining PMMA.

Acknowledgment. The authors thank M. Grunlan for helpful discussions on silane grafting procedures. This research was supported in part by the Robert A. Welch Foundation (A-1585).

Supporting Information Available: Reversible adsorption, patterning, and alignment of microtubules are shown in Supporting Videos 1−3. Supporting Figures S1 and S2 illustrate the proposed route of SAM formation and the relative drag on a microtubule near a surface, respectively. This material is available free of charge *via* the Internet at http://pubs.acs.org.

REFERENCES AND NOTES

1. Guzik, B. W.; Goldstein, L. S. Microtubule-Dependent Transport in Neurons: Steps Towards an Understanding of Regulation, Function and Dysfunction. *Curr. Opin. Cell Biol.* **2004**, *16*, 443–450.
2. Brown, T. B.; Hancock, W. O. A Polarized Microtubule Array for Kinesin-Powered-Nanoscale Assembly and Force Generation. *Nano Lett.* **2002**, *2*, 1131–1135.
3. van den Heuvel, M. G. L.; Dekker, C. Motor Proteins at Work for Nanotechnology. *Science* **2007**, *317*, 333–336.
4. Behrens, S.; Habicht, W.; Wu, J.; Unger, E. Tubulin Assemblies as Biomolecular Templates for Nanostructure Synthesis: From Nanoparticle Arrays to Nanowires. *Surf. Interface Anal.* **2006**, *38*, 1014–1018.
5. Ulman, A. Formation and Structure of Self-Assembled Monolayers. *Chem. Rev.* **1996**, *96*, 1533–1554.
6. Horne, D. S. Casein Structure, Self-Assembly and Gelation. *Curr. Opin. Colloid Interface Sci.* **2002**, *7*, 456–461.
7. Turner, D. C.; Chang, C. Y.; Fang, K.; Brandow, S. L.; Murphy, D. B. Selective Adhesion of Functional Microtubules to Patterned Silane Surfaces. *Biophys. J.* **1995**, *69*, 2782–2789.
8. Boxshall, K.; Wu, M. H.; Cui, Z.; Cui, Z. F.; Watts, J. F.; Baker, M. A. Simple Surface Treatments to Modify Protein Adsorption and Cell Attachment Properties within a Poly(Dimethylsiloxane) Micro-Bioreactor. *Surf. Interface Anal.* **2006**, *38*, 198–201.
9. Sharma, S.; Johnson, R. W.; Desai, T. A. Evaluation of the Stability of Nonfouling Ultrathin Poly(ethylene glycol) Films for Silicon-Based Microdevices. *Langmuir* **2004**, *20*, 348–356.
10. Vermette, P.; Meagher, L. Interactions of Phospholipid- and Poly(ethylene glycol)-Modified Surfaces with Biological Systems: Relation to Physico-Chemical Properties and Mechanisms. *Colloids Surf. B* **2003**, *28*, 153–198.
11. Ariga, K.; Nakanishi, T.; Michinobu, T. Immobilization of Biomaterials to Nano-Assembled Films (Self-Assembled Monolayers, Langmuir−Blodgett Films, and Layer-by-Layer Assemblies) and Their Related Functions. *J. Nanosci. Nanotechnol.* **2006**, *6*, 2278–2301.
12. Senaratne, W.; Andruzzi, L.; Ober, C. K. Self-Assembled Monolayers and Polymer Brushes in Biotechnology: Current Applications and Future Perspectives. *Biomacromolecules* **2005**, *6*, 2427–2448.
13. Ladd, J.; Boozer, C.; Yu, Q.; Chen, S.; Homola, J.; Jiang, S. DNA-Directed Protein Immobilization on Mixed Self-Assembled Monolayers *via* a Streptavidin Bridge. *Langmuir* **2004**, *20*, 8090–8095.
14. Bretagnol, F.; Valsesia, A.; Sasaki, T.; Ceccone, G.; Colpo, P.; Rossi, F. Direct Nanopatterning of 3D Chemically Active Structures for Biological Applications. *Adv. Mater.* **2007**, *19*, 1947.
15. Kannan, B.; Castelino, K.; Chen, F. F.; Majumdar, A. Lithographic Techniques and Surface Chemistries for the Fabrication of PEG-Passivated Protein Microarrays. *Biosens. Bioelectron.* **2006**, *21*, 1960–1967.
16. Muthukrishnan, G.; Roberts, C. A.; Chen, Y. C.; Zahn, J. D.; Hancock, W. O. Patterning Surface-Bound Microtubules through Reversible DNA Hybridization. *Nano Lett.* **2004**, *4*, 2127–2132.
17. Gittes, F.; Meyhofer, E.; Baek, S.; Howard, J. Directional Loading of the Kinesin Motor Molecule as it Buckles a Microtubule. *Biophys. J.* **1996**, *70*, 418–429.
18. Doot, R. K.; Hess, H.; Vogel, V. Engineered Networks of Oriented Microtubule Filaments for Directed Cargo Transport. *Soft Matter* **2007**, *3*, 349–356.
19. Reuther, C.; Hajdo, L.; Tucker, R.; Kasprzak, A. A.; Diez, S. Biotemplated Nanopatterning of Planar Surfaces with Molecular Motors. *Nano Lett.* **2006**, *6*, 2177–2183.
20. Cohen, A. E. Control of Nanoparticles with Arbitrary Two-Dimensional Force Fields. *Phys. Rev. Lett.* **2005**, 94.
21. Cole, M. A.; Voelcker, N. H.; Thissen, H. Electro-Induced Protein Deposition on Low-Fouling Surfaces. *Smart Mater. Struct.* **2007**, *16*, 2222–2228.
22. van den Heuvel, M. G. L.; Butcher, C. T.; Lemay, S. G.; Diez, S.; Dekker, C. Electrical Docking of Microtubules for Kinesin-Driven Motility in Nanostructures. *Nano Lett.* **2005**, *5*, 235–241.
23. Minoura, I.; Muto, E. Dielectric Measurement of Individual Microtubules Using the Electroorientation Method. *Biophys. J.* **2006**, *90*, 3739–3748.
24. Platt, M.; Muthukrishnan, G.; Hancock, W. O.; Williams, M. E. Millimeter Scale Alignment of Magnetic Nanoparticle Functionalized Microtubules in Magnetic Fields. *J. Am. Chem. Soc.* **2005**, *127*, 15686–15687.
25. Huang, Y. M.; Uppalapati, M.; Hancock, W. O.; Jackson, T. N. Microtubule Transport, Concentration and Alignment in Enclosed Microfluidic Channels. *Biomed. Microdevices* **2007**, *9*, 175–184.
26. Yokokawa, R.; Yoshida, Y.; Takeuchi, S.; Kon, T.; Fujita, H. Unidirectional Transport of a Bead on a Single Microtubule Immobilized in a Submicrometre Channel. *Nanotechnology* **2006**, *17*, 289–294.
27. van den Heuvel, M. G. L.; Butcher, C. T.; Smeets, R. M. M.; Diez, S.; Dekker, C. High Rectifying Efficiencies of Microtubule Motility on Kinesin-Coated Gold Nanostructures. *Nano Lett.* **2005**, *5*, 1117–1122.
28. Verma, V.; Hancock, W. O.; Catchmark, J. M. Micro- and Nanofabrication Processes for Hybrid Synthetic and Biological System Fabrication. *IEEE Trans. Adv. Packag.* **2005**, *28*, 584–593.
29. Fischer, T.; Hess, H. Materials Chemistry Challenges in the Design of Hybrid Bionanodevices: Supporting Protein Function within Artificial Environments. *J. Mater. Chem.* **2007**, *17*, 943–951.
30. Norrman, K.; Papra, A.; Kamounah, F. S.; Gadegaard, N.; Larsen, N. B. Quantification of Grafted Poly(ethylene glycol)-Silanes on Silicon by Time-of-Flight Secondary Ion Mass Spectrometry. *J. Mass Spectrom.* **2002**, *37*, 699–708.
31. Shirahata, N.; Hozumi, A. Ultrathin Poly(ethylene glycol) Monolayers Formed by Chemical Vapor Deposition on Silicon Substrates. *J. Nanosci. Nanotechnol.* **2006**, *6*, 1695–1700.
32. Papra, A.; Gadegaard, N.; Larsen, N. B. Characterization of Ultrathin Poly(ethylene glycol) Monolayers on Silicon Substrates. *Langmuir* **2001**, *17*, 1457–1460.
33. Onclin, S.; Ravoo, B. J.; Reinhoudt, D. N. Engineering Silicon Oxide Surfaces Using Self-Assembled Monolayers. *Angew. Chem., Int. Ed.* **2005**, *44*, 6282–6304.
34. Harder, P.; Grunze, M.; Dahint, R.; Whitesides, G. M.; Laibinis, P. E. Molecular Conformation in Oligo(ethylene glycol)-Terminated Self-Assembled Monolayers on Gold and Silver Surfaces Determines Their Ability to Resist Protein Adsorption. *J. Phys. Chem. B* **1998**, *102*, 426–436.
35. Pale-Grosdemange, C.; Simon, E. S.; Prime, K. L.; Whitesides, G. M. Formation of Self-Assembled Monolayers by Chemisorption of Derivatives of Oligo(ethylene glycol) of Structure $HS(CH_2)_{11}(OCH_2CH_2)m$-OH on Gold. *J. Am. Chem. Soc.* **1991**, *113*, 12–20.

36. Satulovsky, J.; Carignano, M. A.; Szleifer, I. Kinetic and Thermodynamic Control of Protein Adsorption. *Proc. Natl. Acad. Sci. U.S.A.* **2000**, *97*, 9037–9041.
37. Unsworth, L. D.; Sheardown, H.; Brash, J. L. Protein-Resistant Poly(ethylene oxide)-Grafted Surfaces: Chain Density-Dependent Multiple Mechanisms of Action. *Langmuir* **2008**, *24*, 1924–1929.
38. Herrwerth, S.; Eck, W.; Reinhardt, S.; Grunze, M. Factors That Determine the Protein Resistance of Oligoether Self-Assembled Monolayers: Internal Hydrophilicity, Terminal Hydrophilicity, and Lateral Packing Density. *J. Am. Chem. Soc.* **2003**, *125*, 9359–9366.
39. Brittain, W. J.; Minko, S. A Structural Definition of Polymer Brushes. *J. Polym. Sci., Part A: Polym. Chem.* **2007**, *45*, 3505–3512.
40. Finocchio, E.; Macis, E.; Raiteri, R.; Busca, G. Adsorption of Trimethoxysilane and of 3-Mercaptopropyltrimethoxysilane on Silica and on Silicon Wafers from Vapor Phase: An Ir Study. *Langmuir* **2007**, *23*, 2505–2509.
41. Owens, T. M.; Ludwig, B. J.; Schneider, K. S.; Fosnacht, D. R.; Orr, B. G.; Holl, M. M. B. Oxidation of Alkylsilane-Based Monolayers on Gold. *Langmuir* **2004**, *20*, 9636–9645.
42. Love, J. C.; Estroff, L. A.; Kriebel, J. K.; Nuzzo, R. G.; Whitesides, G. M. Self-Assembled Monolayers of Thiolates on Metals as a Form of Nanotechnology. *Chem. Rev.* **2005**, *105*, 1103–1169.
43. Hunt, A. J.; Gittes, F.; Howard, J. The Force Exerted by a Single Kinesin Molecule against a Viscous Load. *Biophys. J.* **1994**, *67*, 766–781.
44. Vemparala, S.; Kalia, R. K.; Nakano, A.; Vashishta, P. Electric Field Induced Switching of Poly(ethylene glycol) Terminated Self-Assembled Monolayers: A Parallel Molecular Dynamics Simulation. *J. Chem. Phys.* **2004**, *121*, 5427–5433.
45. Smith, R. K.; Lewis, P. A.; Weiss, P. S. Patterning Self-Assembled Monolayers. *Prog. Surf. Sci.* **2004**, *75*, 1–68.
46. Dennis, J. R.; Howard, J.; Vogel, V. Molecular Shuttles: Directed Motion of Microtubules Slang Nanoscale Kinesin Tracks. *Nanotechnology* **1999**, *10*, 232–236.
47. Fadley, C. S. Angle-Resolved X-ray Photoelectron-Spectroscopy. *Prog. Surf. Sci.* **1984**, *16*, 275–388.